Nano Research 2018, 11(10): 5615–5628
https://doi.org/10.1007/s12274-018-2107-8
Research Article
ISSN 1998-0124
CN 11-5974/O4

The shape effect of reconstituted high-density lipoprotein nanocarriers on brain delivery and Aβ clearance

Huahua Song[1,§], Xinyi Ma[1,§], Jianrong Xu[1,§], Qingxiang Song[1], Meng Hu[1,3], Xiao Gu[1], Qian Zhang[1], Lina Hou[1], Lepei Chen[1], Yukun Huang[2], Ping Yu[1], Dayuan Wang[1], Gan Jiang[1], Meng Huang[1], Jun Chen[2], Hongzhuan Chen[1] (✉), and Xiaoling Gao[1] (✉)

[1] *Department of Pharmacology and Chemical Biology, Faculty of Basic Medicine, School of Medicine, Shanghai Jiao Tong University, Shanghai 200025, China*
[2] *Key Laboratory of Smart Drug Delivery, Ministry of Education, School of Pharmacy, Fudan University, Lane 826, Zhangheng Road, Shanghai 201203, China*
[3] *Department of Pharmacy, Ren Ji Hospital, School of Medicine, Shanghai Jiao Tong University, Shanghai 200127, China*
[§] *Huahua Song, Xinyi Ma, and Jianrong Xu contributed equally to this work.*

Received: 14 March 2018
Revised: 21 May 2018
Accepted: 24 May 2018

KEYWORDS
reconstituted high density lipoprotein,
β-amyloid,
apolipoprotein E,
spherical,
discoidal,
Alzheimer's disease

ABSTRACT

Accumulation of extracellular β-amyloid (Aβ) is crucial for the pathogenesis of Alzheimer's disease (AD), and the development of novel therapeutic agents that can both accelerate Aβ clearance and inhibit the subsequent pathological cascades is regarded as a promising strategy for AD management. In our previous study, we have constructed discoidal apolipoprotein E3–reconstituted high-density lipoprotein (ApoE3-rHDL) as an efficient nanoplatform that can penetrate the blood–brain barrier and accelerate Aβ clearance for a combination treatment of AD. To further improve its drug loading capacity, we hypothesized that spherical rHDL might serve as a more powerful nanocarrier if it has the same brain delivery and Aβ clearance abilities as the discoidal rHDL does. To evaluate the potential of spherical rHDL as a promising alternative for the combination therapy for AD, here, we investigated the effect of the shape of rHDL on its brain delivery, Aβ clearance, and anti-AD efficacy. We found that spherical rHDL had stronger Aβ-binding affinity than discoidal rHDL did, more effectively facilitated microglial uptake and degradation of $A\beta_{1-42}$, achieved better brain distribution after intravenous administration, and more powerfully reduced Aβ deposition, decreased microglia activation, attenuated neurological damage, and rescued memory deficits in a mouse model of AD. Among the rHDLs evaluated, monosialotetrahexosyl ganglioside–incorporated spherical rHDL exerted the best effect. The findings of this study for the first time show a shape effect of an rHDL nanocarrier on its biological functions and suggest that a spherical lipoprotein-mimic nanocarrier may serve as a more efficient multifunctional nanoplatform for AD therapy.

Address correspondence to Hongzhuan Chen, hongzhuan_chen@hotmail.com; Xiaoling Gao, shellygao1@sjtu.edu.cn

1 Introduction

High-density lipoprotein (HDL), a natural nanoparticle and the smallest lipoprotein, plays a well-recognized biological role and is highly suitable as a nanoplatform for medical diagnostics and therapeutics [1–3]. To produce them on a large scale and to prevent blood-borne pollution, HDLs had been successfully reconstructed to serve as nanomedicines because they exert a biological action or facilitate targeted drug delivery [4–6]. Just as natural HDL, discoidal and spherical reconstituted HDLs (rHDLs) have been developed for such biomedical applications [4–7]. Nonetheless, the shape effect of rHDL on its biological functions has hardly been explored [8, 9].

Alzheimer's disease (AD) is the most common form of dementia and imposes a heavy medical and economic burden on modern society [10]. Accumulation of extracellular β-amyloid (Aβ) is crucial for AD pathogenesis, and the common late-onset form of AD is characterized by an overall impairment of Aβ clearance [11–14]. In addition, it has been widely acknowledged that the secondary pathological processes—such as neuroinflammation, formation of neurofibrillary tangles, synapse dysfunction, and neuron loss—can independently increase the severity of AD, once they are initiated by Aβ aggregation [15–17]. Thus, the development of novel therapeutic agents that can both accelerate Aβ clearance and inhibit other subsequent pathological cascades is regarded as a promising strategy for AD management [18].

By mimicking HDL in the central nervous system (CNS), in our previous work, we constructed apolipoprotein E3–reconstituted high-density lipoprotein (ApoE3-rHDL) as an efficient nanoplatform that can penetrate the blood–brain barrier (BBB) and accelerate Aβ clearance to serve as a novel nanomedicine for the treatment of AD [19, 20]. By incorporating monosialotetrahexosyl ganglioside (GM1) into the lipid membrane of ApoE3-rHDL, we next designed GM1-rHDL, which possessed antibody-like strong binding affinity for Aβ, more effectively facilitated microglia-mediated Aβ degradation and Aβ efflux across the BBB, and simultaneously allowed for effective loading of a neuroprotective peptide, as a nanoplatform for the combination therapy for AD [21]. Nevertheless, these rHDL nanocarriers are both discoidal in shape and allow for drug loading only via insertion into the lipid membrane or via conjugation with the surface components of rHDL. Therefore, these rHDLs can achieve only low loading capacity, limited drug protection, and may even compromise the targeting property of the nanocarriers. In contrast, spherical rHDL with a core can provide additional space for drug loading not only for hydrophobic but also for hydrophilic agents [22–24] and thus may serve as an attractive alternative for the combination treatment of AD.

To evaluate the potential of spherical rHDL as a promising alternative for the combination treatment of AD, it is critical to investigate the shape effect of rHDL on its brain delivery, Aβ-binding affinity, and Aβ clearance capacity. To achieve this goal, here we constructed two discoidal rHDL nanocarriers (d-rHDL and d-GM1-rHDL) and two corresponding spherical rHDL nanocarriers (s-rHDL and s-GM1-rHDL). We evaluated their brain delivery capacity by determining their binding affinity for low-density lipoprotein receptor (LDLR, the major receptor on the BBB that mediates the blood-to-brain transcytosis of rHDL [25–28]), their cellular uptake in bEnd.3 cells (a mouse brain microvascular endothelial cell line), and their brain distribution following intravenous administration. We then compared their capacity for Aβ clearance by detecting their binding affinity for both the Aβ monomer and oligomer, evaluated their effect on microglia-mediated cellular uptake and degradation of Aβ, and determined their effect on AD-related neuropathology and cognitive deficits.

2 Experimental

2.1 Materials

1,2-dimyristoyl-sn-glycero-3-phosphocholine (DMPC) and GM1 were acquired from Avanti Polar Lipids (Alabaster, AL, USA). Full-length ApoE3 was provided by Peprotech (Rocky Hill, NJ, USA). $A\beta_{1-42}$, 1,1′-dioctadecyl-3,3,3′,3′-tetramethylindocarbocyanine perchlorate (DiI), 1,1-dioctadecyl-3,3,3,3-tetramethylindotricarbocyanine iodide (DiR), and Aβ enzyme-linked immunosorbent assay (ELISA) kits were

purchased from Invitrogen (Carlsbad, CA, USA). FAM-Aβ_{1-42} was provided by AnaSpec (Fremont, CA, USA). All cell culture reagents were bought from Gibco (Grand Island, NY, USA) unless indicated otherwise.

2.2 Cell lines

BV2 cells and bEnd.3 cells were provided by the Cell Institute of the Chinese Academy of Sciences (Shanghai, China) and were cultured in Dulbecco's modified Eagle's medium (DMEM) supplemented with 10% of fetal bovine serum (FBS), 100 U·mL^{-1} penicillin, and 2 mM Gluta MAX-I supplement at 37 ℃ in a humidified atmosphere containing 5% of CO_2.

2.3 Animals

Senescence-accelerated mouse resistant 1 (SAMR1) and senescence-accelerated mouse prone 8 (SAMP8) mice were obtained from the Animal Center of the First Affiliated Hospital of Tianjin University of Traditional Chinese Medicine. The animals were housed at a specific pathogen-free animal facility with free access to food and water. The protocol of the animal experiment was approved by the Animal Experimentation Ethics Committee, Shanghai Jiao Tong University School of Medicine.

2.4 Preparation and characterization of d-rHDL, s-rHDL, d-GM1-rHDL, and s-GM1-rHDL

d-rHDL composed of DMPC and ApoE3 and d-GM1-rHDL consisting of DMPC, GM1, and ApoE3 were prepared as described previously [19, 21]. s-rHDL and s-GM1-rHDL were prepared by the same protocol by adding cholesterol oleate (3:100, mass ratio of cholesterol oleate to total lipid) to the lipid mixture for the preparation of d-rHDL and d-GM1-rHDL, respectively [29]. DiI, DiR-labeled d-rHDL, s-rHDL, d-GM1-rHDL, and s-GM1-rHDL were prepared in a similar manner except that DiI (1% to DMPC, w/w) and DiR (1% to DMPC, w/w) were included for preparation of the lipid film. Zetasizer Nano-ZS90 (Malvern Instruments, UK) was used to measure the zeta potential and size distributions of d-rHDL, s-rHDL, d-GM1-rHDL, and s-GM1-rHDL. Transmission electron microscopy (TEM), cryo-scanning electron microscopy (Cryo-SEM), and atomic force microscopy (AFM) were carried out to characterize the morphology and structure of the nanoparticles. For TEM analysis, the samples were subjected to negative staining with 1.75% phosphotungstic acid and then examined under a Hitachi H-7650 transmission electron microscope (Hitachi, Inc., Japan). For Cryo-SEM analysis, the samples were prepared by means of a VITROBOT automated Cryo-SEM sample preparation unit (FEI, Holland) and stored in liquid nitrogen until imaging. The images were acquired using an FEI TECNAI G2 electron microscope (FEI, Holland) at 200 kV and 160 ℃. For AFM analysis, the samples were dried on mica film before scanning, and the images were obtained via Multimode NanoScope Ⅲa (Bruker, Germany).

The DMPC concentration of these nanoparticles was determined via liquid chromatography with mass spectrometry (Shimazhu 20AD-AB Sciex 4000 Mass Spectrometer) on a phenyl column with methanol: 0.1% formamide buffer (pH 3.0) (98:2) as the mobile phase at the flow rate of 0.4 mL·min^{-1} with an ESI source in positive ion mode. The curtain gas was set to 10 psi, ion source gas 1 to 50 psi, and ion source gas 2 to 50 psi. The needle voltage was 4,500 V, gas temperature 600 ℃, collision gas 20 psi, decluttering potential 170 V, and collision energy 41 V. Multiple reaction monitoring (MRM) mode was chosen for the detection of DMPC via the transition of m/z from 678.5 to 184.1.

2.5 Preparation of Aβ_{1-42} monomer and oligomer

Aβ_{1-42} was dissolved in hexafluoro-2-isopropanol at 1 mg·mL^{-1} and stored at –20 ℃. Before use, hexafluoro-2-isopropanol was evaporated, and the peptide was resuspended in dimethyl sulfoxide (DMSO) at a concentration of 5 mM and was water bath–sonicated for 10 min to obtain a monomeric preparation. For the preparation of the Aβ_{1-42} oligomer, monomeric peptide DMSO solution (5 mM) was diluted to 100 μM with deionized water and incubated at 4 ℃ for 24 h. The presence of the oligomer in these preparations has been previously confirmed and characterized [30].

2.6 Surface plasmon resonance (SPR) analysis

This analysis was performed on a Biacore T200

instrument (GE Healthcare, USA). LDLR was immobilized onto an NTA chip. Phosphate buffer (PBS) (0.01 M, pH 7.4) served as a buffer solution. LDLR solution at 2 μg·mL^{-1} was injected for 20 s at a flow rate of 5 μL·min^{-1}. The upstream parallel flow cell was blank (filled with PBS). The binding of different groups was conducted in PBS (0.01 M, pH 7.4) with the analytes (containing 0–100 nM ApoE3) injected into the flow system at a flow rate of 30 μL·min^{-1}. Dissociation was conducted in the same buffer for 30 min, and the chip was then regenerated with 0.5% SDS for 30 s, then with 350 mM EDTA for 30 s. Calculation of the kinetic constants of binding was performed in the BIA evaluation software using the 1:1 Langmuir binding model. d-rHDL, s-rHDL, d-GM1-rHDL, and s-GM1-rHDL served as the analytes.

The Aβ_{1-42} monomer and oligomer were immobilized to a CM5 chip (RU, 2,000) as previously described [20]. A parallel flow channel that was activated by EDC/NHS and then blocked with 1 M ethanolamine served as the reference channel. Experiments were conducted with sterile PBS (pH 7.4) as running buffer, and an analyte was injected at a flow rate of 30 μL·min^{-1}. A series of concentrations of d-rHDL, s-rHDL, d-GM1-rHDL, and s-GM1-rHDL (diluted in 0.01 M PBS, pH 7.4) was injected into the flow system, and the kinetic constants of binding were obtained using a 1:1 Langmuir binding model via the BIA evaluation software.

2.7 Uptake of Aβ by BV2 cells in the presence of d-rHDL, s-rHDL, d-GM1-rHDL, or s-GM1-rHDL

BV2 cells, a mouse brain microglial cell line, were employed to evaluate the effect of the shape on rHDL-facilitated cellular uptake of FAM-Aβ_{1-42}. The cells were seeded at 5 × 10^3 cells per well in 96-well plates, allowed to grow for 24 h, and then exposed to a series of concentrations of DiI-labeled d-rHDL, s-rHDL, d-GM1-rHDL, or s-GM1-rHDL.

For a quantitative experiment, d-rHDL, s-rHDL, d-GM1-rHDL, and s-GM1-rHDL were diluted to the DMPC concentration of 0.25, 0.5, 1, and 2 μg·mL^{-1}. After incubation with the different concentrations of d-rHDL, s-rHDL, d-GM1-rHDL, or s-GM1-rHDL for 1 h, the cells were coincubated with 2 μg·mL^{-1} FAM-Aβ_{1-42} for 3 h. Then, the cells were washed twice with PBS, fixed in 4% formaldehyde for 15 min at 37 ℃, stained with Hoechst 33258 for 15 min at room temperature, and then subjected to the analysis under a High Content Kinetic Scan (HCS) Reader (Thermo Scientific, USA). The cellular uptake data were normalized for comparison by setting the data obtained from d-rHDL (0.5 μg·mL^{-1}) to 1.0.

2.8 Intracellular Aβ degradation in BV2 cells in the presence of d-rHDL, s-rHDL, d-GM1-rHDL, or s-GM1-rHDL

To reveal the possible promoting effect of d-rHDL, s-rHDL, d-GM1-rHDL, and s-GM1-rHDL on cellular degradation of Aβ, BV2 cells were seeded in 96-well plates at a density of 5 ×10^3 cells per well, allowed to grow for 24 h, and then were exposed to 0.5 μg·mL^{-1} (DMPC concentration) of d-rHDL, s-rHDL, d-GM1-rHDL, or s-GM1-rHDL. After incubation for 1 h, the cells were coincubated with 2 μg·mL^{-1} Aβ for 3 h. After a wash with PBS, the cells were lysed in 1% SDS containing a protease inhibitor cocktail (Roche, Switzerland). The total protein content of cell lysates was analyzed by a bicinchoninic acid (BCA) protein assay (Thermo, USA). The remaining intracellular Aβ_{1-42} levels were quantified with an ELISA kit (Invitrogen, USA) and normalized to total protein of the lysates [31].

2.9 Brain distribution of d-rHDL, s-rHDL, d-GM1-rHDL, and s-GM1-rHDL following intravenous administration

Twenty nude mice were randomly distributed into four groups, and intravenously injected with DiR-labeled d-rHDL, s-rHDL, d-GM1-rHDL, or s-GM1-rHDL. The fluorescent images were captured at 30 min, 1, 2, 4, and 24 h after injection with the CRi Maestro® *in vivo* fluorescence imaging system (CRi, MA, USA). Four hours after administration, three mice of each group were committed to collection of different organs and were imaged.

2.10 Immunohistochemical analysis

Following 4-week treatment with d-rHDL, s-rHDL,

d-GM1-rHDL, or s-GM1-rHDL at the DMPC dose of 1 mg·kg^{-1}, the mice were anesthetized, and the heart was perfused with cold saline. The brains were collected and fixed in 4% paraformaldehyde, embedded in paraffin, and sectioned at 4 μm. For immunohistochemical analysis, the slides were incubated in 70% citric acid for 3 min, and then in methanol containing 1% peroxide for 10 min. After microwave treatment in distilled water for 3 min, the slides were blocked for 1 h in a 20% normal goat serum solution containing 0.1% of Triton X-100, and then incubated with a primary antibody in the blocking solution overnight at 4 ˚C. The 6E10 antibody against Aβ was used to stain Aβ plaques, and the IBA1 antibody to stain the activated microglia [32]. The antigens were detected by means of secondary antibodies by standard ABC-DAB methods; the images were captured via a microscope (Leica DM2500P with Leica DFC320 digital camera) and analyzed in the Image Pro-Plus software (Media Cybernetics, Silver Spring, MD).

The brain sections were stained with cresyl violet or hematoxylin–eosin (H&E) in accordance with a standard protocol and then subjected to examination under a Leica microscope. Nissl staining sections served for determination of neuronal injury in the cortex and in the CA1 region and the dentate gyrus (DG) region of the hippocampus. H&E-stained sections were subjected to robust examination of the morphological changes in the hippocampus.

2.11 The Morris water maze (MWM) test

The MWM test was performed as described elsewhere to evaluate the spatial learning and memory of AD model mice [33]. After the 4-week treatment with d-rHDL, s-rHDL, d-GM1-rHDL, or s-GM1-rHDL at the DMPC dose of 1 mg·kg^{-1}, the mice were trained four times a day for five days. A computer-controlled tracking system (Shanghai Jiliang Software Technology Co., Ltd.) was implemented to record the escape latency and swimming route. On the sixth day, with the platform removed, the mice were placed into the tank from the same fixed positions and allowed to swim freely for 60 s, with the times of platform crossing recorded.

2.12 Statistical analysis

The data were expressed as mean ± standard deviation (SD). Differences between two groups were evaluated by two-tailed Student's t test, and among multiple groups by one-way ANOVA followed by Bonferroni's test. Statistical significance was defined as $p < 0.05$.

3 Results and discussion

3.1 Preparation and characterization of discoidal and spherical rHDLs

d-rHDL and d-GM1-rHDL were prepared by incubating ApoE3 with DMPC liposomes or GM1-DMPC liposomes, respectively, according to our previously reported method [21]. s-rHDL and s-GM1-rHDL were prepared by the same procedure by adding cholesterol oleate to form the core of spherical rHDL. DiI or DiR (at 1% of DMPC, w/w) was incorporated into the membrane of d-rHDL, d-GM1-rHDL, s-rHDL, and s-GM1-rHDL for fluorescent labeling. The size distributions of d-rHDL, d-GM1-rHDL, s-rHDL, and s-GM1-rHDL were determined by dynamic light scattering (DLS), and the particle size was found to be 27.42 ± 9.70 (mean ± SD), 28.68 ± 3.65, 26.03 ± 3.26, and 26.38 ± 5.66 nm, respectively (Fig. 1, Table 1). The zeta potential of GM1-modified formulations, i.e., d-GM1-rHDL (–35.18 ± 0.78 mV) and s-GM1-rHDL (–33.65 ± 0.29 mV), was more negative than that of d-rHDL (–9.83 ± 0.45 mV) and s-rHDL (–7.87 ± 0.16 mV; Table 1), thus indicating effective incorporation of GM1, an anionic amphiphilic glycolipid, into the lipid membrane. Fluorescent labeling hardly changed either the size or the zeta potential of d-rHDL, d-GM1-rHDL, s-rHDL, and s-GM1-rHDL (Table S1 in the Electronic Supplementary Material (ESM)). TEM analysis revealed that d-rHDL, d-GM1-rHDL, s-rHDL, and s-GM1-rHDL generally had a circular shape with a diameter ~ 20 nm (Fig. 1). Cryo-SEM and AFM analyses confirmed the discoidal shape (with a stick projection) of d-rHDL and d-GM1-rHDL and the spherical shape (with a circle projection) of s-rHDL and s-GM1-rHDL.

3.2 Discoidal and spherical rHDLs show similar binding affinity for LDLR

Accessing the brain is one of the major properties for

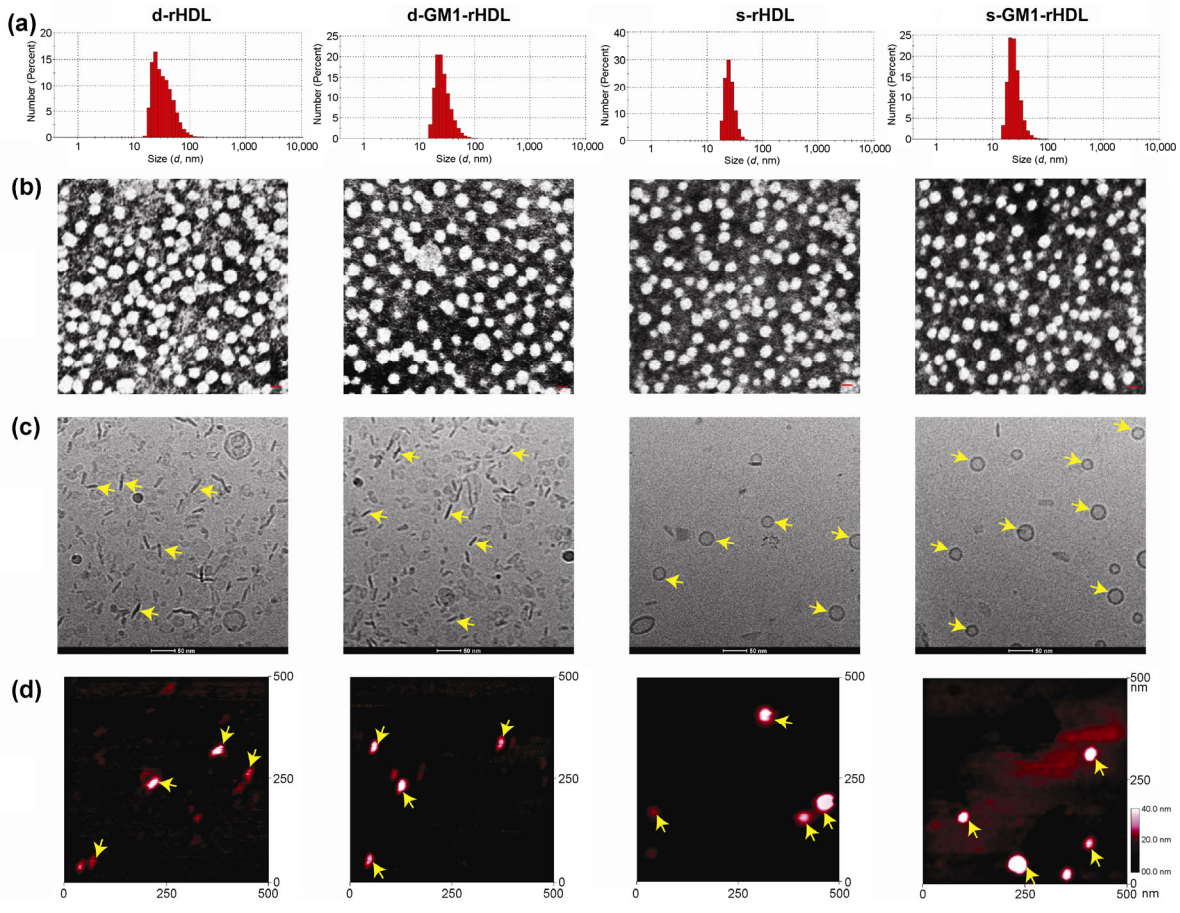

Figure 1 Particle size, morphology, and structures of the four groups of nanoparticles. (a) Size distribution of d-rHDL, d-GM1-rHDL, s-rHDL, and s-GM1-rHDL measured by DLS on a Zetasizer. (b) Morphology of d-rHDL, d-GM1-rHDL, s-rHDL, and s-GM1-rHDL observed by TEM after negative staining with phosphotungstic acid (1.75%, w/v) (scale bar = 50 nm). (c) The structure of d-rHDL, d-GM1-rHDL, s-rHDL, and s-GM1-rHDL was examined by Cryo-SEM (scale bar = 50 nm). (d) AFM images of d-rHDL, d-GM1-rHDL, s-rHDL, and s-GM1-rHDL.

Table 1 Particle sizes and zeta potentials of nanoparticles

Nanoparticle	PDI[a]	Particle size (*d*, nm)	Zeta potential (mV)
d-rHDL	0.24	27.42 ± 9.70	−9.83 ± 0.45
s-rHDL	0.24	26.03 ± 3.26	−7.87 ± 0.16
d-GM1-rHDL	0.26	28.68 ± 3.65	−35.18 ± 0.78
s-GM1-rHDL	0.26	26.38 ± 5.66	−33.65 ± 0.29

[a] PDI, polydispersity index.

nanoparticles to exert their therapeutic effects in the CNS. ApoE nanoparticles have been shown to cross the BBB via LDLR-mediated transcytosis [19, 22, 34, 35]. Therefore, it is crucial to determine the LDLR recognition capacity of different nanoparticles. Here, SPR analysis was performed to characterize the LDLR-binding affinity of the discoidal and spherical rHDLs. Previous work revealed that one LDLR can bind to one ApoE-containing nanoparticle [36]. Even when there may be several ApoE molecules on a single nanoparticle, the steric effects of both the nanoparticles and the dextran matrix of the chip surface would not allow one nanoparticle to bind to several ligands simultaneously. Therefore, as in previous work [36, 37], we utilized the 1:1 Langmuir binding model to analyze the interaction between LDLR and rHDLs. As presented in Fig. 2, d-rHDL, d-GM1-rHDL, s-rHDL, and s-GM1-rHDL showed similar binding curves and binding affinity constants (K_D) toward LDLR (0.47, 0.39, 0.30, and 0.43 nM, respectively), suggesting that the discoidal and spherical rHDLs possessed similar binding affinity for LDLR.

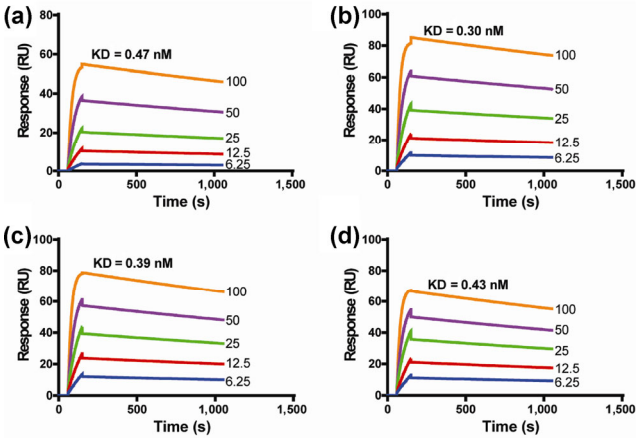

Figure 2 SPR analysis of the ApoEconcentration-dependent binding of LDLR. Concentration-dependent curves of binding of (a) d-rHDL, (b) s-rHDL, (c) d-GM1-rHDL, and (d) s-GM1-rHDL to LDLR. The kinetic constants of binding were calculated by means of the BIA evaluation software using the 1:1 Langmuir binding model.

3.3 The brain delivery efficiency of discoidal and spherical rHDLs

Sequentially, we determined the effect of the shape on the brain delivery of the various nanoparticles by evaluating their uptake by bEnd.3 cells (a mouse brain endothelial cell line [38]) and found that the cellular uptake of spherical rHDL was slightly higher than that of discoidal rHDL (Fig. 3(a)). At the concentration of total lipid of 0.5, 4, and 20 μg·mL^{-1}, the uptake of s-rHDL by bEnd.3 cells was 35.93%, 6.47%, and 18.53% higher than that of d-rHDL, respectively. Accordingly, at the concentration of total lipid 0.5, 4, and 20 μg·mL^{-1}, the cellular uptake of s-GM1-rHDL was 62.94%, 44.84%, and 27.23% higher than that of d-GM1-rHDL, respectively. Some investigators found that the spherical nanoparticles need to overcome a minimal membrane-bending energy barrier, as compared with their nonspherical counterparts, whereas internalization of disk-like nanoparticles involves a strong membrane deformation, responsible for a large free energy barrier [39]. The above SPR analysis revealed that discoidal and spherical rHDLs possessed similar binding affinity for LDLR; therefore, we assumed that the difference in the membrane-bending energy barrier between discoidal and spherical rHDLs could be the major reason for their difference in cellular uptake.

We then evaluated the brain delivery efficiency of the different nanoparticles after intravenous administration, where d-rHDL, s-rHDL, d-GM1-rHDL, and s-GM1-rHDL were fluorescently labeled with DiR (characterization of size and zeta potential is shown in Table 1). As shown in Figs. 3(b) and 3(c), a slightly greater fluorescent signal of DiR was observed in the brains after the administration of spherical rHDLs (s-rHDL or s-GM1-rHDL) than that after the treatment with discoidal rHDLs (d-rHDL or d-GM1-rHDL), suggesting that the brain delivery of spherical rHDLs was slightly higher than that of discoidal rHDLs. The higher cellular internalization efficiency of spherical rHDLs in the brain endothelial cells might be the major cause of such difference.

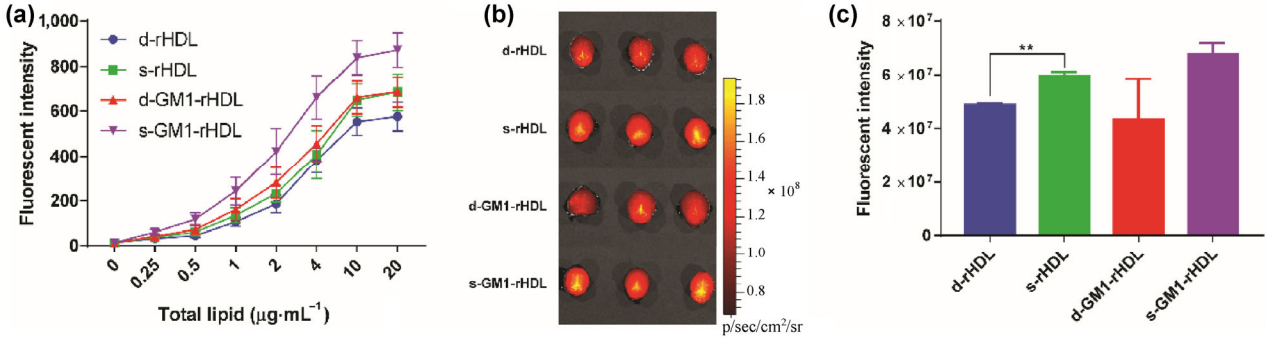

Figure 3 (a) High-content scanning quantitative analysis of concentration-dependent cellular uptake of DiI-d-rHDL, DiI-s-rHDL, DiI-d-GM1-rHDL, and DiI-s-GM1-rHDL after incubation with bEnd.3 cells at 37 ˚C for 3 h. (b) Accumulation of DiR-d-rHDL, DiR-s-rHDL, DiR-d-GM1-rHDL, and DiR-s-GM1-rHDL in the brain of mice at 4 h after intravenous administration; $n = 3$. (c) Quantitative accumulation of DiR-d-rHDL, DiR-s-rHDL, DiR-d-GM1-rHDL, and DiR-s-GM1-rHDL in the brain of mice at 4 h after intravenous administration; $n = 3$, $^{**}p < 0.01$.

3.4 Spherical rHDLs show higher binding affinity for the Aβ monomer and oligomer

One of the most important mechanisms underlying the rHDL-mediated Aβ clearance is the binding to Aβ and facilitation of its cellular uptake and degradation in microglia [19, 21]. $Aβ_{1–40}$ and $Aβ_{1–42}$ are the most common sequential proteolytic byproducts of amyloid β-protein precursor (APP) [40, 41]. Although $Aβ_{1–40}$ constitutes ~ 90% of the cleaved form of APP, $Aβ_{1–42}$ has a greater propensity to aggregate and plays a critical role in the initiation of plaque formation and AD pathogenesis [42–44]. Aggregates of $Aβ_{1–42}$ (protofibrils and fibrils) have also been reported to be more toxic to cultured neurons than $Aβ_{1–40}$ aggregates are [45–47]. Here, to compare the effectiveness of discoidal rHDLs and spherical rHDLs at facilitating Aβ clearance, we first compared the binding affinity between the rHDL nanocarriers and the $Aβ_{1–42}$ monomer or oligomer (the soluble Aβ species). For this analysis, the $Aβ_{1–42}$ monomer and oligomer were separately immobilized on two separate flow cells of a CM5 chip via an amino coupling reaction as described elsewhere [21]. The reference flow cell was blocked with ethanolamine immediately after activation. An ApoE concentration–dependent binding process was recorded after the application of d-rHDL, s-rHDL, d-GM1-rHDL, or s-GM1-rHDL. As compared with d-rHDL (K_D = 4.85 ± 2.91 and 7.93 ± 0.98 nM, respectively), s-rHDL (K_D = 2.21 ± 0.76 and 2.34 ± 0.33 nM, respectively) showed stronger binding affinity for the Aβ monomer and oligomer. As in our previous study, incorporation of GM1 enhanced the Aβ-binding affinity of rHDL [21]. Moreover, s-GM1-rHDL (K_D = 0.79 ± 0.74 and 0.32 ± 0.43 nM, respectively) also showed stronger Aβ-binding affinity than did d-GM1-rHDL (K_D = 0.95 ± 0.87 and 0.88 ± 0.49 nM, respectively; Fig. 4). Some studies have shown that the interaction between ApoE and Aβ depends on the ApoE isotype and conformation [48]. Lipidation of ApoE increases its affinity for Aβ 5- to 10-fold by changing the conformation of ApoE [49]. Here, we found that spherical rHDLs have stronger binding affinity for Aβ than do their corresponding discoidal controls. This phenomenon could be caused by the increased curvature of the spherical structures that changes the conformation of ApoE and better presents its Aβ-binding site.

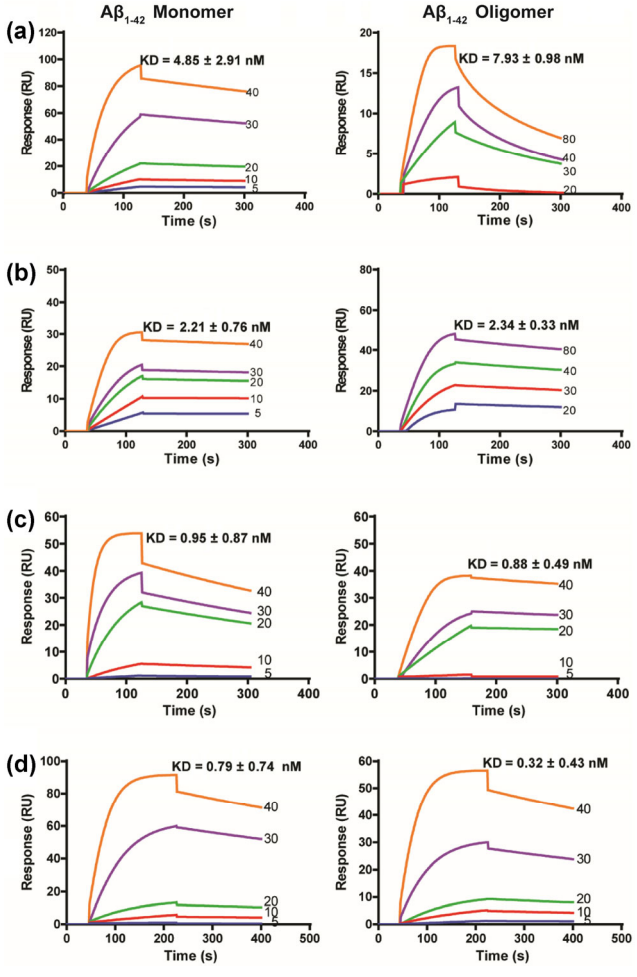

Figure 4 SPR analysis of the ApoE concentration–dependent binding of (a) d-rHDL, (b) s-rHDL, (c) d-GM1-rHDL, or (d) s-GM1-rHDL to the $Aβ_{1–42}$ monomer and oligomer. The kinetic constants of binding were calculated with the BIA evaluation software by using the 1:1 Langmuir binding model, n = 3.

3.5 Spherical rHDLs more effectively facilitate microglial cellular uptake and degradation of $Aβ_{1–42}$

It is well known that several Aβ clearance pathways likely exist in the CNS, including proteolytic digestion, efflux across the BBB, and bulk flow drainage of interstitial fluid and cerebrospinal fluid [50]. Nanoparticles possessing Aβ-binding affinity have an ability to accelerate cell-based proteolytic digestion of Aβ [19, 21]. s-GM1-rHDL, which manifested the strongest Aβ-binding affinity, was expected to effectively accelerate Aβ clearance via the above mechanisms.

Owing to the high affinity for both LDLR and Aβ, we assumed that this binding would promote cellular uptake. BV2 cells (a mouse microglia cell line) served as a cell model to verify the relation between high affinity and nanoparticle-facilitated cellular uptake and degradation of Aβ [51]. As illustrated in Fig. 5, consistent with the trend of Aβ-binding affinity, spherical rHDLs (s-rHDL and s-GM1-rHDL) more effectively enhanced the cellular uptake and degradation of Aβ when compared with the discoidal rHDLs (d-rHDL and d-GM1-rHDL). s-GM1-rHDL, which manifested the strongest Aβ-binding affinity, showed the highest Aβ uptake and degradation efficiency.

3.6 Spherical rHDLs more effectively reduce Aβ deposition, decrease microglia activation, attenuate neurological damage, and reverse memory deficits in AD model mice

We then performed immunohistochemical analysis to evaluate the ability of d-rHDL, s-rHDL, d-GM1-rHDL, and s-GM1-rHDL to reduce Aβ deposition and microglia activation. As indicated in Fig. 6, compared with NaCl (the negative control), all the four rHDLs dramatically reduced both types of Aβ plaques. Specifically, the amount of Aβ plaques in the brains of the s-rHDL-treated mice was 33.16% lower than that in the brains of the d-rHDL-treated animals. Likewise, the amount of Aβ plaques in the brain of s-GM1-rHDL–treated mice was 24.70% lower than that in the d-GM1-rHDL–treated mice. We did not determine the binding affinity of rHDLs for the

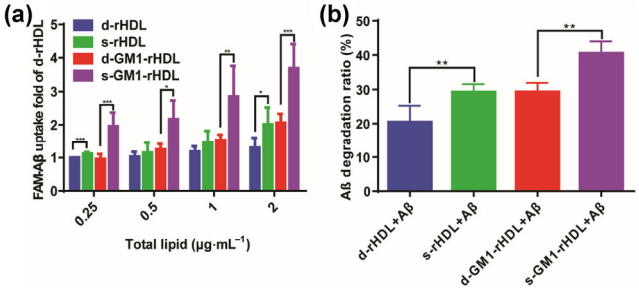

Figure 5 Spherical rHDLs promote cellular uptake and degradation of Aβ. (a) Cellular uptake of $Aβ_{1–42}$ in the presence of d-rHDL, s-rHDL, d-GM1-rHDL, and s-GM1-rHDL; the d-rHDL group was set to 100%. (b) ELISA results on cell degradation of $Aβ_{1–42}$ in the presence of d-rHDL, s-rHDL, d-GM1-rHDL, or s-GM1-rHDL at total lipid concentration of 0.5 μg·mL^{-1}; *p < 0.05, **p < 0.01, ***p < 0.001.

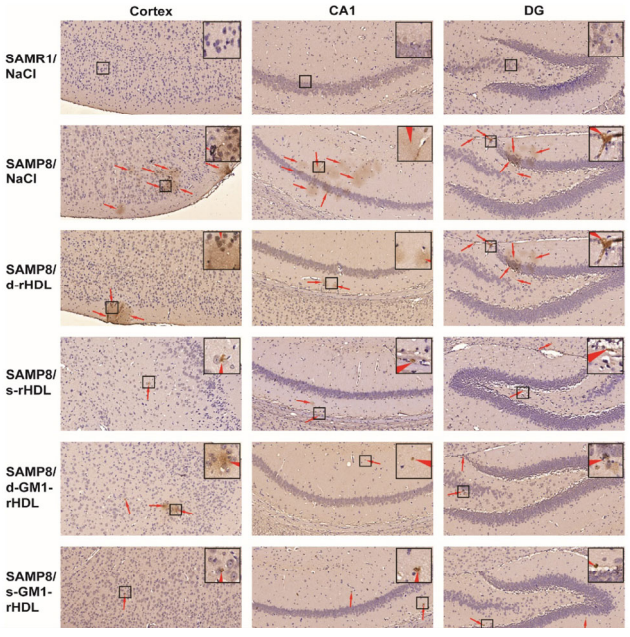

Figure 6 The effect of d-rHDL, s-rHDL, d-GM1-rHDL, or s-GM1-rHDL on the clearance of Aβ plaques in brains of SAMP8 mice. Eight-month-old SAMP8 mice (n = 3) received 4-week daily intravenous injections of d-rHDL, s-rHDL, d-GM1-rHDL, or s-GM1-rHDL at the DMPC dose of 1 mg·kg^{-1}. Age-matched SAMP8 and SAMR1 mice dosed with normal saline served as the negative and normal control, respectively. The brain sections (4 μm) were immunostained with an anti-Aβ antibody (6E10) and quantitatively analyzed in the Image Pro-Plus software. Scale bar, 100 μm.

Aβ fibril (i.e., the major component of Aβ plaques). Nevertheless, such significantly reduced amounts of Aβ plaques in both the cortex and hippocampus after the rHDL treatment suggested that, just as the multifunctional nanoplatforms reported previously [52, 53], rHDLs may also induce Aβ disaggregation and degradation. The higher Aβ clearance efficiency of spherical rHDLs could be caused by their elevated efficiency of brain delivery, higher binding affinity for the Aβ monomer and oligomer, and greater capacity for facilitating microglia-mediated Aβ uptake and degradation. Such clearance of the soluble form of Aβ (Aβ monomer and oligomer) thus effectively induces disaggregation and degradation of Aβ fibrils to remove intracerebral Aβ plaques. The reduced Aβ burden thus decreased microglia activation. As shown in Fig. 7, the level of microglia activation in the brain of s-rHDL-treated mice was 27.55% less than that in d-rHDL-treated mice. Likewise, the level of microglia activation in the s-GM1-rHDL–treated mice was 27.98%

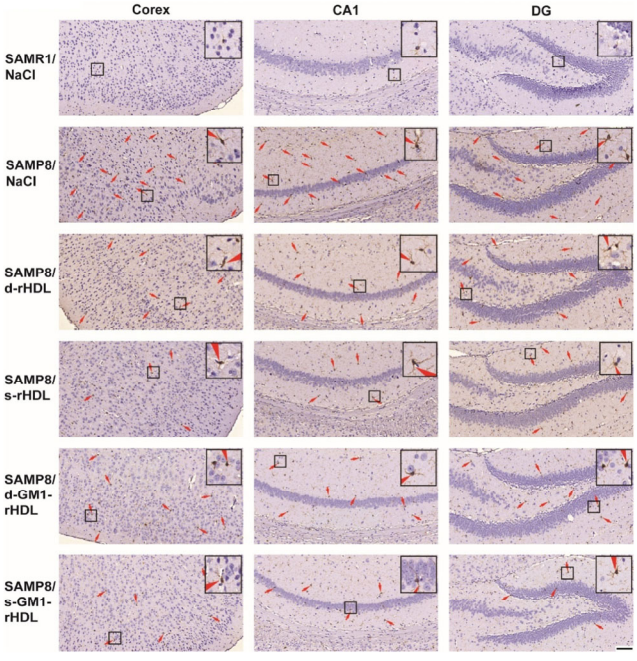

Figure 7 The negative effect of d-rHDL, s-rHDL, d-GM1-rHDL, or s-GM1-rHDL on microglia activation in the brain of SAMP8 mice. Eight-month-old SAMP8 mice (n = 3) received 4-week daily intravenous injections of d-rHDL, s-rHDL, d-GM1-rHDL, or s-GM1-rHDL at the DMPC dose of 1 mg·kg^{-1}. Age-matched SAMP8 and SAMR1 mice dosed with normal saline served as the negative and normal control, respectively. The brain sections (4 μm) were immunostained with an anti-IBA1 antibody and quantitatively analyzed in the Image Pro-Plus software. Scale bar, 100 μm.

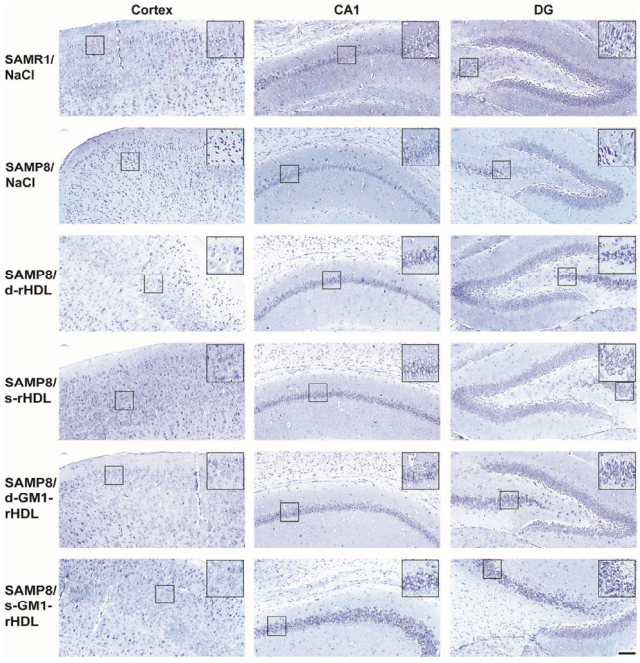

Figure 8 The neuroprotective effects of d-rHDL, s-rHDL, d-GM1-rHDL, and s-GM1-rHDL as evidenced by Nissl staining. Eight-month-old SAMP8 mice (n = 3) received 4-week daily intravenous injections of d-rHDL, s-rHDL, d-GM1-rHDL, or s-GM1-rHDL at the DMPC dose of 1 mg·kg^{-1}. Age-matched SAMP8 and SAMR1 mice dosed with normal saline served as the negative and normal control, respectively. The brain sections (4 μm) were immunostained with Nissl reagents. Scale bar, 100 μm.

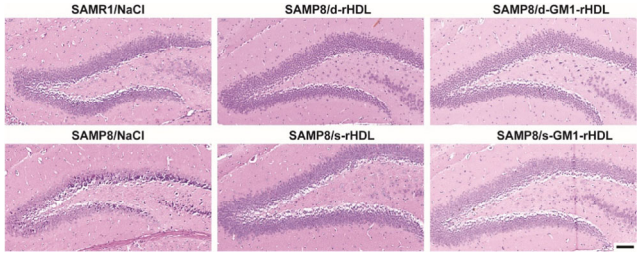

Figure 9 The neuroprotective effects of d-rHDL, s-rHDL, d-GM1-rHDL, and s-GM1-rHDL as determined by H&E staining. Eight-month-old SAMP8 mice (n = 3) received 4-week daily intravenous injections of d-rHDL, s-rHDL, d-GM1-rHDL, or s-GM1-rHDL at the DMPC dose of 1 mg·kg^{-1}. Age-matched SAMP8 and SAMR1 mice dosed with normal saline served as the negative and normal control, respectively. The brain sections (4 μm) were immunostained with H&E reagents. Scale bar, 100 μm.

less than that in the d-GM1-rHDL–treated mice (Fig. S1 in the ESM).

Moreover, the neuroprotective effects of d-rHDL, s-rHDL, d-GM1-rHDL, and s-GM1-rHDL were evaluated morphologically after Nissl staining and H&E staining (Figs. 8 and 9). It was found that Nissl bodies in the cortex and in the CA1 and DG regions of the hippocampus of the animals treated with rHDLs were much denser and more organized than those in the mice injected with NaCl. Spherical rHDLs more effectively attenuated neurological damage than the discoidal rHDLs did, and the animals treated with s-GM1-rHDL showed the greatest alleviation of neuronal damage.

Spherical rHDLs more effectively reduced Aβ deposition, decreased microglia activation, and attenuated neurological damage. These changes should therefore improve the spatial learning and memory of AD model animals. As revealed by the MWM test (Fig. 10), compared with the SAMP8 mice treated with NaCl (i.e., the negative control AD model mice [54, 55]), all the animals treated with rHDLs showed attenuation of memory deficits. Compared with discoidal-rHDL–treated mice, spherical-rHDL–treated animals manifested lesser memory loss, and the animals

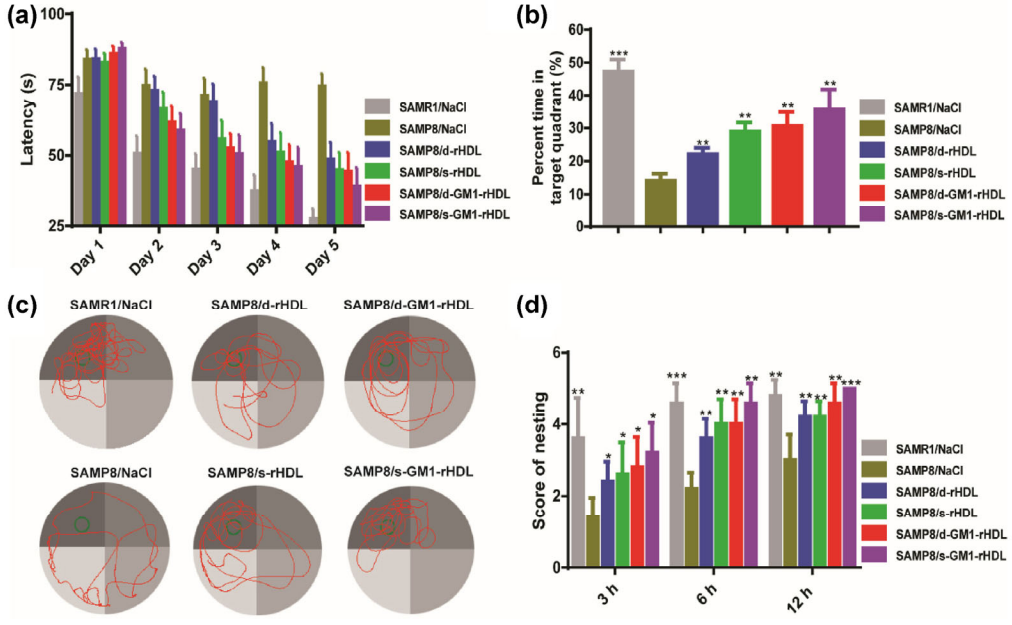

Figure 10 The alleviating effect of d-rHDL, s-rHDL, d-GM1-rHDL, or s-GM1-rHDL on memory deficits in AD model mice as evidenced by the MWM test and nesting test. Eight-month-old SAMP8 mice (n = 3) received 4-week daily intravenous injections of d-rHDL, s-rHDL, d-GM1-rHDL, or s-GM1-rHDL at the DMPC dose of 1 mg·kg^{-1}. Age-matched SAMP8 and SAMR1 mice dosed with normal saline served as the negative and normal control, respectively. (a) Latency time. (b) The percentage of time spent in the target quadrant. (c) A typical swimming path. (d) The nesting score. Data are presented as mean ± SEM; n = 6; *p < 0.05, **p < 0.01 significantly different from that of the SAMP8/NaCl group.

treated with s-GM1-rHDL behaved the best in terms of learning performance with shortest latency (Fig. 10(a)) and spent the longest time in the target quadrant after removal of the hidden platform (Fig. 10(b)). The representative swimming paths are depicted in Fig. 10(c). In addition, as revealed by a nesting test, as expected, these s-GM1-rHDL-treated mice showed higher nest construction capability than did the animals treated with the other formulations (Fig. 10(d) and Fig. S2 in the ESM).

4 Conclusions

In summary, we focused on the effect of the shape of rHDL on its brain delivery, Aβ clearance, and AD severity. We found that spherical rHDLs manifested stronger Aβ-binding affinity than discoidal rHDLs did, more effectively accelerated their cellular uptake and $A\beta_{1-42}$ degradation in microglia, achieved a better brain distribution after intravenous administration, and more strongly reduced Aβ deposition, decreased microglia activation, alleviated neurological deterioration, and reversed memory impairments in AD model mice. Among the rHDLs evaluated, GM1-containing spherical rHDL exerted the best effect. The findings of this work for the first time reveal the shape effect of an rHDL nanocarrier on its biological functions and suggest that spherical lipoprotein-mimic nanocarriers hold great potential as a more effective multifunctional nanoplatform for AD therapy.

Acknowledgements

This work was supported by the National Natural Science Foundation of China (Nos. 81373351, 81573382, 81722043, and 81503174), the National Science and Technology Major Project (No. 2018ZX09734005-007), the National Youth Talent Support Program, grant from Shanghai Science and Technology Committee (No. 15540723700), and "Shu Guang" project supported by Shanghai Municipal Education Commission and Shanghai Education Development Foundation (No. 15SG14).

Electronic Supplementary Material: Supplementary material (further details of particle size and zeta

potential of DiI/DiR-nanoparticles, quantitative data of Aβ plaques and activated microglia in d-rHDL, s-rHDL, d-GM1-rHDL and s-GM1-rHDL groups of mice brains, nesting results of d-rHDL, s-rHDL, d-GM1-rHDL and s-GM1-rHDL groups of mice) is available in the online version of this article at https://doi.org/10.1007/s12274-018-2107-8.

References

[1] Kuai, R.; Li, D.; Chen, Y. E.; Moon, J. J.; Schwendeman, A. High-density lipoproteins: Nature's multifunctional nanoparticles. *ACS Nano* **2016**, *10*, 3015–3041.

[2] Mo, Z. C.; Ren, K.; Liu, X.; Tang, Z. L.; Yi, G. H. A high-density lipoprotein-mediated drug delivery system. *Adv. Drug Deliv. Rev.* **2016**, *106*, 132–147.

[3] Damiano, M. G.; Mutharasan, R. K.; Tripathy, S.; McMahon, K. M.; Thaxton, C. S. Templated high density lipoprotein nanoparticles as potential therapies and for molecular delivery. *Adv. Drug Deliv. Rev.* **2013**, *65*, 649–662.

[4] Bricarello, D. A.; Smilowitz, J. T.; Zivkovic, A. M.; German, J. B.; Parikh, A. N. Reconstituted lipoprotein: A versatile class of biologically-inspired nanostructures. *ACS Nano* **2011**, *5*, 42–57.

[5] Thaxton, C. S.; Rink, J. S.; Naha, P. C.; Cormode, D. P. Lipoproteins and lipoprotein mimetics for imaging and drug delivery. *Adv. Drug Deliv. Rev.* **2016**, *106*, 116–131.

[6] Simonsen, J. B. Evaluation of reconstituted high-density lipoprotein (rHDL) as a drug delivery platform-a detailed survey of rHDL particles ranging from biophysical properties to clinical implications. *Nanomedicine* **2016**, *12*, 2161–2179.

[7] Huang, H.; Cruz, W.; Chen, J.; Zheng, G. Learning from biology: Synthetic lipoproteins for drug delivery. *Wiley Interdiscip. Rev.: Nanomed. Nanobiotechnol.* **2015**, *7*, 298–314.

[8] Zhang, W. L.; He, H. L.; Liu, J. P.; Wang, J.; Zhang, S. Y.; Zhang, S. S.; Wu, Z. M. Pharmacokinetics and atherosclerotic lesions targeting effects of tanshinone II–A discoidal and spherical biomimetic high density lipoproteins. *Biomaterials* **2013**, *34*, 306–319.

[9] Zhang, W. L.; Xiao, Y.; Liu, J. P.; Wu, Z. M.; Gu, X.; Xu, Y. M.; Lu, H. Structure and remodeling behavior of drug-loaded high density lipoproteins and their atherosclerotic plaque targeting mechanism in foam cell model. *Int. J. Pharm.* **2011**, *419*, 314–321.

[10] Hebert, L. E.; Weuve, J.; Scherr, P. A.; Evans, D. A. Alzheimer disease in the United States (2010–2050) estimated using the 2010 census. *Neurology* **2013**, *80*, 1778–1783.

[11] Wang, J.; Gu, B. J.; Masters, C. L.; Wang, Y. J. A systemic view of Alzheimer disease-insights from amyloid-β metabolism beyond the brain. *Nat. Rev. Neurol.* **2017**, *13*, 612–623.

[12] Kurochkin, I. V.; Guarnera, E.; Berezovsky, I. N. Insulin-degrading enzyme in the fight against Alzheimer's disease. *Trends Pharmacol. Sci.* **2018**, *39*, 49–58.

[13] Villemagne, V. L.; Doré, V.; Burnham, S. C.; Masters, C. L.; Rowe, C. C. Imaging tau and amyloid-β proteinopathies in Alzheimer disease and other conditions. *Nat. Rev. Neurol.* **2018**, *14*, 225–236.

[14] Lee, S. J. C.; Nam, E.; Lee, H. J.; Savelieff, M. G.; Lim, M. H. Towards an understanding of amyloid-β oligomers: Characterization, toxicity mechanisms, and inhibitors. *Chem. Soc. Rev.* **2017**, *46*, 310–323.

[15] Hyman, B. T. Amyloid-dependent and amyloid-independent stages of Alzheimer disease. *Arch. Neurol.* **2011**, *68*, 1062–1064.

[16] Heneka, M. T.; Golenbock, D. T.; Latz, E. Innate immunity in Alzheimer's disease. *Nat. Immunol.* **2015**, *16*, 229–236.

[17] Reiss, A. B.; Arain, H. A.; Stecker, M. M.; Siegart, N. M.; Kasselman, L. J. Amyloid toxicity in Alzheimer's disease. *Rev. Neurosci.*, in press, DOI: 10.1515/revneuro-2017-0063.

[18] Sevigny, J.; Chiao, P.; Bussière, T.; Weinreb, P. H.; Williams, L.; Maier, M.; Dunstan, R.; Salloway, S.; Chen, T.; Ling, Y. et al. The antibody aducanumab reduces Aβ plaques in Alzheimer's disease. *Nature* **2016**, *537*, 50–56.

[19] Song, Q. X.; Huang, M.; Yao, L.; Wang, X. L.; Gu, X.; Chen, J.; Chen, J.; Huang, J. L.; Hu, Q. Y.; Kang, T. et al. Lipoprotein-based nanoparticles rescue the memory loss of mice with Alzheimer's disease by accelerating the clearance of amyloid-beta. *ACS Nano* **2014**, *8*, 2345–2359.

[20] Song, Q. X.; Song, H. H.; Xu, J. R.; Huang, J. L.; Hu, M.; Gu, X.; Chen, J.; Zheng, G.; Chen, H. Z.; Gao, X. L. Biomimetic ApoE-reconstituted high density lipoprotein nanocarrier for blood-brain barrier penetration and amyloid beta-targeting drug delivery. *Mol. Pharm.* **2016**, *13*, 3976–3987.

[21] Huang, M.; Hu, M.; Song, Q. X.; Song, H. H.; Huang, J. L.; Gu, X.; Wang, X. L.; Chen, J.; Kang, T.; Feng, X. Y. et al. GM1-modified lipoprotein-like nanoparticle: Multifunctional nanoplatform for the combination therapy of Alzheimer's disease. *ACS Nano* **2015**, *9*, 10801–10816.

[22] Huang, J. L.; Jiang, G.; Song, Q. X.; Gu, X.; Hu, M.; Wang, X. L.; Song, H. H.; Chen, L. P.; Lin, Y. Y.; Jiang, D. et al. Lipoprotein-biomimetic nanostructure enables efficient targeting delivery of siRNA to *Ras*-activated glioblastoma cells via macropinocytosis. *Nat. Commun.* **2017**, *8*, 15144.

[23] Schwendeman, A.; Sviridov, D. O.; Yuan, W. M.; Guo,

Y. H.; Morin, E. E.; Yuan, Y.; Stonik, J.; Freeman, L.; Ossoli, A.; Thacker, S. et al. The effect of phospholipid composition of reconstituted HDL on its cholesterol efflux and anti-inflammatory properties. *J. Lipid Res.* **2015**, *56*, 1727–1737.

[24] Gentile, F.; Chiappini, C.; Fine, D.; Bhavane, R. C.; Peluccio, M. S.; Cheng, M. M. C.; Liu, X.; Ferrari, M.; Decuzzi, P. The effect of shape on the margination dynamics of non-neutrally buoyant particles in two-dimensional shear flows. *J. Biomech.* **2008**, *41*, 2312–2318.

[25] Molino, Y.; David, M.; Varini, K.; Jabès, F.; Gaudin, N.; Fortoul, A.; Bakloul, K.; Masse, M.; Bernard, A.; Drobecq, L. et al. Use of LDL receptor-targeting peptide vectors for *in vitro* and *in vivo* cargo transport across the blood-brain barrier. *FASEB J.* **2017**, *31*, 1807–1827.

[26] Basak, J. M.; Verghese, P. B.; Yoon, H.; Kim, J.; Holtzman, D. M. Low-density lipoprotein receptor represents an apolipoprotein E-independent pathway of Aβ uptake and degradation by astrocytes. *J. Biol. Chem.* **2012**, *287*, 13959–13971.

[27] Wang, D. R.; El-Amouri, S. S.; Dai, M.; Kuan, C. Y.; Hui, D. Y.; Brady, R. O.; Pan, D. Engineering a lysosomal enzyme with a derivative of receptor-binding domain of apoE enables delivery across the blood-brain barrier. *Proc. Natl. Acad. Sci. USA* **2013**, *110*, 2999–3004.

[28] Prévost, M.; Raussens, V. Apolipoprotein E-low density lipoprotein receptor binding: Study of protein-protein interaction in rationally selected docked complexes. *Proteins* **2004**, *55*, 874–884.

[29] Rajora, M. A.; Ding, L.; Valic, M.; Jiang, W.; Overchuk, M.; Chen, J.; Zheng, G. Tailored theranostic apolipoprotein E3 porphyrin-lipid nanoparticles target glioblastoma. *Chem. Sci.* **2017**, *8*, 5371–5384.

[30] Stine, W. B., Jr.; Dahlgren, K. N.; Krafft, G. A.; LaDu, M. J. *In vitro* characterization of conditions for amyloid-β peptide oligomerization and fibrillogenesis. *J. Biol. Chem.* **2003**, *278*, 11612–11622.

[31] Robert, J.; Stukas, S.; Button, E.; Cheng, W. H.; Lee, M.; Fan, J. J.; Wilkinson, A.; Kulic, I.; Wright, S. D.; Wellington, C. L. Reconstituted high-density lipoproteins acutely reduce soluble brain Aβ levels in symptomatic APP/PS1 mice. *Biochim. Biophys. Acta* **2016**, *1862*, 1027–1036.

[32] Chiu, I. M.; Phatnani, H.; Kuligowski, M.; Tapia, J. C.; Carrasco, M. A.; Zhang, M.; Maniatis, T.; Carroll, M. C. Activation of innate and humoral immunity in the peripheral nervous system of ALS transgenic mice. *Proc. Natl. Acad. Sci. USA* **2009**, *106*, 20960–20965.

[33] Yao, L.; Gu, X.; Song, Q. X.; Wang, X. L.; Huang, M.; Hu, M.; Hou, L. N.; Kang, T.; Chen, J.; Chen, H. Z. et al. Nanoformulated alpha-mangostin ameliorates Alzheimer's disease neuropathology by elevating LDLR expression and accelerating amyloid-beta clearance. *J. Control. Release* **2016**, *226*, 1–14.

[34] Portioli, C.; Bovi, M.; Benati, D.; Donini, M.; Perduca, M.; Romeo, A.; Dusi, S.; Monaco, H. L.; Bentivoglio, M. Novel functionalization strategies of polymeric nanoparticles as carriers for brain medications. *J. Biomed. Mater. Res. A* **2017**, *105*, 847–858.

[35] Ćurić, A.; Möschwitzer, J. P.; Fricker, G. Development and characterization of novel highly-loaded itraconazole poly(butyl cyanoacrylate) polymeric nanoparticles. *Eur. J. Pharm. Biopharm.* **2017**, *114*, 175–185.

[36] Calabuig-Navarro, M. V.; Jackson, K. G.; Kemp, C. F.; Leake, D. S.; Walden, C. M.; Lovegrove, J. A.; Minihane, A. M. A randomized trial and novel SPR technique identifies altered lipoprotein-LDL receptor binding as a mechanism underlying elevated LDL-cholesterol in APOE4s. *Sci. Rep.* **2017**, *7*, 44119.

[37] Tassa, C.; Duffner, J. L.; Lewis, T. A.; Weissleder, R.; Schreiber, S. L.; Koehler, A. N.; Shaw, S. Y. Binding affinity and kinetic analysis of targeted small molecule-modified nanoparticles. *Bioconjug. Chem.* **2010**, *21*, 14–19.

[38] Yin, T. T.; Yang, L. C.; Liu, Y.; Zhou, X. B.; Sun, J.; Liu, J. Sialic acid (SA)-modified selenium nanoparticles coated with a high blood-brain barrier permeability peptide-B6 peptide for potential use in Alzheimer's disease. *Acta Biomater.* **2015**, *25*, 172–183.

[39] Li, Y.; Kröger, M.; Liu, W. K. Shape effect in cellular uptake of PEGylated nanoparticles: Comparison between sphere, rod, cube and disk. *Nanoscale* **2015**, *7*, 16631–16646.

[40] Goedert, M. NEURODEGENERATION. Alzheimer's and Parkinson's diseases: The prion concept in relation to assembled Aβ, tau, and α-synuclein. *Science* **2015**, *349*, 1255555.

[41] Goldstein, L. E.; Muffat, J. A.; Cherny, R. A.; Moir, R. D.; Ericsson, M. H.; Huang, X. D.; Mavros, C.; Coccia, J. A.; Faget, K. Y.; Fitch, K. A. et al. Cytosolic β-amyloid deposition and supranuclear cataracts in lenses from people with Alzheimer's disease. *Lancet* **2003**, *361*, 1258–1265.

[42] Jarrett, J. T.; Lansbury, P. T., Jr. Seeding "one-dimensional crystallization" of amyloid: A pathogenic mechanism in Alzheimer's disease and scrapie? *Cell* **1993**, *73*, 1055–1058.

[43] Colvin, M. T.; Silvers, R.; Ni, Q. Z.; Can, T. V.; Sergeyev, I.; Rosay, M.; Donovan, K. J.; Michael, B.; Wall, J.; Linse, S. et al. Atomic resolution structure of monomorphic $A\beta_{42}$ amyloid fibrils. *J. Am. Chem. Soc.* **2016**, *138*, 9663–9674.

[44] He, Z. H.; Guo, J. L.; McBride, J. D.; Narasimhan, S.; Kim, H.; Changolkar, L.; Zhang, B.; Gathagan, R. J.; Yue, C. Y.; Dengler, C. et al. Amyloid-β plaques enhance Alzheimer's

brain tau-seeded pathologies by facilitating neuritic plaque tau aggregation. *Nat. Med.* **2018**, *24*, 29–38.

[45] Dahlgren, K. N.; Manelli, A. M.; Stine, W. B., Jr.; Baker, L. K.; Krafft, G. A.; LaDu, M. J. Oligomeric and fibrillar species of amyloid-β peptides differentially affect neuronal viability. *J. Biol. Chem.* **2002**, *277*, 32046–32053.

[46] Jan, A.; Gokce, O.; Luthi-Carter, R.; Lashuel, H. A. The ratio of monomeric to aggregated forms of Abeta40 and Abeta42 is an important determinant of amyloid-beta aggregation, fibrillogenesis, and toxicity. *J. Biol. Chem.* **2008**, *283*, 28176–28189.

[47] Colvin, M. T.; Silvers, R.; Frohm, B.; Su, Y. C.; Linse, S.; Griffin, R. G. High resolution structural characterization of $A\beta_{42}$ amyloid fibrils by magic angle spinning NMR. *J. Am. Chem. Soc.* **2015**, *137*, 7509–7518.

[48] Yu, J. T.; Tan, L.; Hardy, J. Apolipoprotein E in Alzheimer's disease: An update. *Annu. Rev. Neurosci.* **2014**, *37*, 79–100.

[49] Tokuda, T.; Calero, M.; Matsubara, E.; Vidal, R.; Kumar, A.; Permanne, B.; Zlokovic, B.; Smith, J. D.; Ladu, M. J.; Rostagno, A. et al. Lipidation of apolipoprotein E influences its isoform-specific interaction with Alzheimer's amyloid beta peptides. *Biochem. J.* **2000**, *348*, 359–365.

[50] Kurz, A.; Perneczky, R. Amyloid clearance as a treatment target against Alzheimer's disease. *J. Alzheimers Dis.* **2011**, *24*, 61–73.

[51] Feng, C. Z.; Yin, J. B.; Yang, J. J.; Cao, L. Regulatory factor X1 depresses ApoE-dependent Aβ uptake by miRNA-124 in microglial response to oxidative stress. *Neuroscience* **2017**, *344*, 217–228.

[52] Li, M.; Yang, X. J.; Ren, J. S.; Qu, K. G.; Qu, X. G. Using graphene oxide high near-infrared absorbance for photothermal treatment of Alzheimer's disease. *Adv. Mater.* **2012**, *24*, 1722–1728.

[53] Guan, Y. J.; Li, M.; Dong, K.; Gao, N.; Ren, J. S.; Zheng, Y. C.; Qu, X. G. Ceria/POMs hybrid nanoparticles as a mimicking metallopeptidase for treatment of neurotoxicity of amyloid-β peptide. *Biomaterials* **2016**, *98*, 92–102.

[54] Butterfield, D. A.; Poon, H. F. The senescence-accelerated prone mouse (SAMP8): A model of age-related cognitive decline with relevance to alterations of the gene expression and protein abnormalities in Alzheimer's disease. *Exp. Gerontol.* **2005**, *40*, 774–783.

[55] Akiguchi, I.; Pallàs, M.; Budka, H.; Akiyama, H.; Ueno, M.; Han, J. X.; Yagi, H.; Nishikawa, T.; Chiba, Y.; Sugiyama, H. et al. SAMP8 mice as a neuropathological model of accelerated brain aging and dementia: Toshio Takeda's legacy and future directions. *Neuropathology* **2017**, *37*, 293–305.